Solid State Science and Technology, Vol. 19, No2 (2011) 80-91
ISSN 0128-7389

CHARACTERIZATION OF Yb-DOPED $Ba(Ce,Zr)O_3$ NANOPOWDERS PREPARED BY PECHINI METHOD

N. Osman[1]*, I. A. Talib[2] and H. A. Hamid[1]

[1]*Fakulti Sains Gunaan, Universiti Teknologi MARA, 02600 Arau, Perlis*

[2]*Pusat Pengajian Fizik Gunaan, Fakulti Sains & Teknologi, Universiti Kebangsaan Malaysia, 43600 Bangi, Selangor*

**Corresponding author: fisha@ perlis.uitm.edu.my*

ABSTRACT

Ceramic compounds of $Ba(Ce_{1-x}Zr_x)_{0.95}Yb_{0.05}O_{2.975}$; x=0.20, 0.30, 0.40, 0.50 and 0.60 were successfully prepared by a Pechini method using metal-nitrate salts as starting materials. The samples were characterized by XRD, particle analyzer, SEM and impedance spectroscopy (IS). It was found that annealing temperature of 1400 to 1450 ^oC is sufficient to produce pure perovskite-like phase with a single structure. Particles size distribution and scanning electron micrographs revealed that the size of the loose powder particles was in nanosize range (50-200 nm). The increase in Zr content reduced the size of the loose powders and they tend to form agglomerates. Sintered at $T \geq 1400$ ^oC, samples with x=0.20, 0.30 and 0.40 showed density ≥ 93% of the theoretical. The samples formed clear and compact grains with submicron sizes. On the other hand, samples with x=0.5 and 0.6 exhibited low relative density (< 80%) with smaller grains size. This observation might be due to the agglomerates effect. Proton conductivities of the $Ba(Ce_{1-x}Zr_x)_{0.95}Yb_{0.05}O_{2.975}$; x=0.20, 0.30 and 0.40 were measured by impedance spectroscopy between 200 to 800 ^oC in wet hydrogen. The results showed that the grain semicircle was observed only at $T \leq 250$ ^oC. This phenomenon limits the grain resistance (R_g) data and it was found that the R_g data points deviated from the linearity of Arrhenius behaviour. Thus, only total conduction was discussed in this study.

Keywords: cerate-zirconate; nanopowders; grain size; electrical conductivity; activation energy;

INTRODUCTION

Studies on the cerate-zirconate ceramics that combine the high conductivity of cerates and the high chemical stability of zirconates have been widely reported in literatures [1-3]. The compounds were prepared by substituting zirconium at cerium-sites or cerium at zirconium-sites to form cation B^{4+} in perovskite ceramics ABO_3. The materials are very promising candidates as solid electrolytes in a variety of electrochemical devices such as solid oxide fuel cells (SOFCs) and gas sensors [4]. Various Zr concentrations,

ranging from 5 to 90 mol% substituted Ce-sites or Ce at Zr-sites have been reported in literatures [5-7]. However, to maintain chemical stability towards CO_2 derived from zirconate base and the high electrical conductivity derived from cerate base, the required Zr-content in the range 20 to 60 mol% are needed [3, 8].

It is generally understood that in these oxides, the preparation process plays an important role in the mechanical and electrical properties of the final sintered ceramic products. It has been proven that wet chemical methods (WCMs) such as Pechini method can produce powders and dense compacted powders at temperature lower than that used in solid state reaction method (SSR) [9]. Based on the trends, this work was carried out to prepare and characterize a polycrystalline ceramic of $Ba(Ce_{1-x}Zr_x)_{0.95}Yb_{0.05}O_{2.975}$; x=0.20, 0.30, 0.40, 0.50 and 0.60.

EXPERIMENTAL DETAILS

Stoichiometric amounts of metal nitrate salts such as $Ce(NO_3)_3.6H_2O$, $Ba(NO_3)_2$, $Yb(NO_3)_3.5H_2O$ and $ZrO(NO_3)_2$. $4.84H_2O$ were dissolved in distilled water and continuously stirred by a magnetic stirrer to make a transparent nitrate solution. Citric acid (CA) was first added into the nitrate solution followed by ethylene glycol (EG) under continuous stirring. Then a concentrated ammonia solution was gradually added into the mixture. The resulting solution was heated and stirred continuously using a hot-plate and a magnetic stirrer until a viscous clear solution of metal-citrate complexes was obtained. The gel was dried on a hot-plate overnight and transformed to a dark gray sponge-like material. The sponge-like was pre-calcined in a furnace at 550 ^oC for 5 h. The as-calcined powder was then calcined at 1100 ^oC for 27 h to produce light yellow powders.

The calcined powder was pressed under a pressure of 5 tons for 5 min to become a pellet. The pellet was sintered at 1400-1450 ^oC in air for 6 h. For impedance conductivity measurement, Pt paste was painted onto opposite surfaces of the pellet as electrodes and then heated at 1000 ^oC in air for 5 h.

The samples were characterized by a X-ray diffractometer (Bruker D8 Advanced) (Cu-K_α; λ=1.5418 Å) from 20 to 80^o in steps of 0.025^o, a laser scattering particle size distribution analyzer model Malvern Nano S (ZEN 1600) and a scanning electron microscope (SEM) model Leo 1450 VP. The impedance of the samples in wet hydrogen was measured using a High Frequency Response Analyzer (HFRA), Solartron 1260. Impedance spectra were recorded from 200 to 800 ^oC in frequency range from 1 Hz to 10 MHz. The impedance spectra were analyzed to extract the grain (*g*) and grain-boundary (*gb*) responses using a Z-View program (Scribner Associates, Inc).

A detailed samples preparation method as well as characterization techniques have been reported in our previous work [10].

Solid State Science and Technology, Vol. 19, No2 (2011) 80-91
ISSN 0128-7389

RESULTS AND DISCUSSION

Phase Identification

Figure 1 shows the XRD pattern for the powders of $Ba(Ce_{1-x}Zr_x)_{0.95}Yb_{0.05}O_{2.975}$ samples after calcined at 1100 ^oC for 27 h. All the samples almost formed a single perovskite-phase with ortorombic structure for x=0.20 and cubic structure for x=0.30, 0.40, 0.50 and 0.60. The presence of a small $BaCO_3$ peak at $2\theta \approx 24^o$ indicates that the carbonate contamination still remains in the samples. The existence of this impurity phase causes to the formation of small fluorite structure such as $(Ce,Zr)O_2$ in the sample. Therefore, higher temperature is still needed to obtain high purity of samples based on cerate-zirconate compared to the cerate [11] or zirconate [12] ceramics.

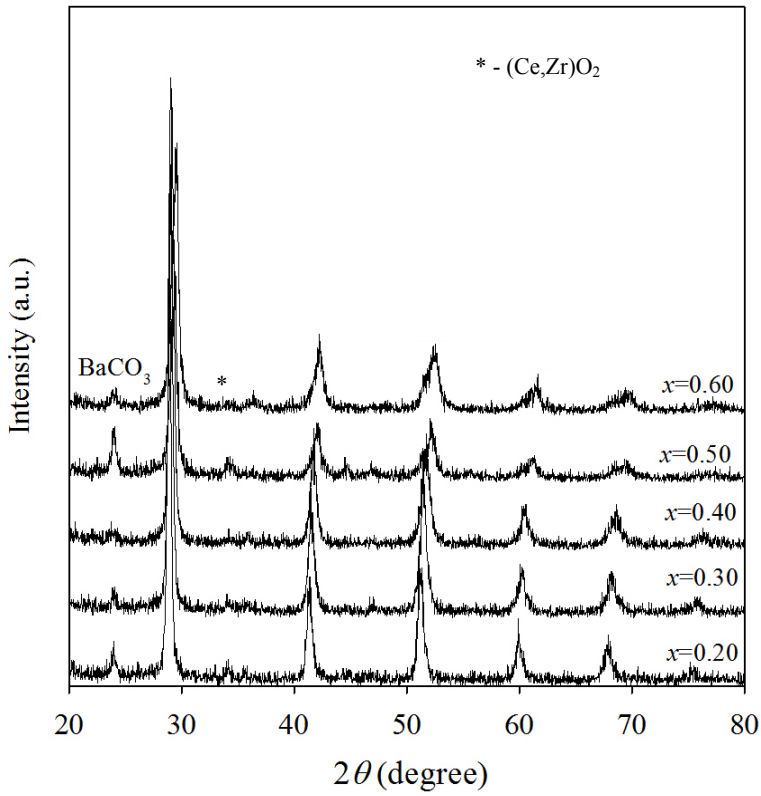

Figure 1: XRD pattern for $Ba(Ce_{1-x}Zr_x)_{0.95}Yb_{0.05}O_{2.975}$ after the samples in the form of powders were calcined at 1100 ^oC for 27 h

To become a good ceramics electrolyte, besides the high crystallinity, the samples also must exhibit very dense solid compounds. Thus, all the samples were sintered in the form of pellets at T=1400-1450 ^oC for 6 h. Figure 2 shows the XRD spectra for the sintered pellets of $Ba(Ce_{1-x}Zr_x)_{0.95}Yb_{0.05}O_{2.975}$. All the pellet surfaces were polished prior to the XRD measurement as suggested by Magrez and Schober [13]. It can be clearly seen that the background signal became relatively lower and the sharper peaks appeared. Up to x=0.4, $BaCO_3$ traces were not detected in the samples. The absence of

this carbonate residue was also proven by FTIR as reported previously [10]. The densities of the pellets also achieved more than 90%. However, for x=0.50 and x=0.60, the samples show lower purity and their density is 85% and 60%, respectively.

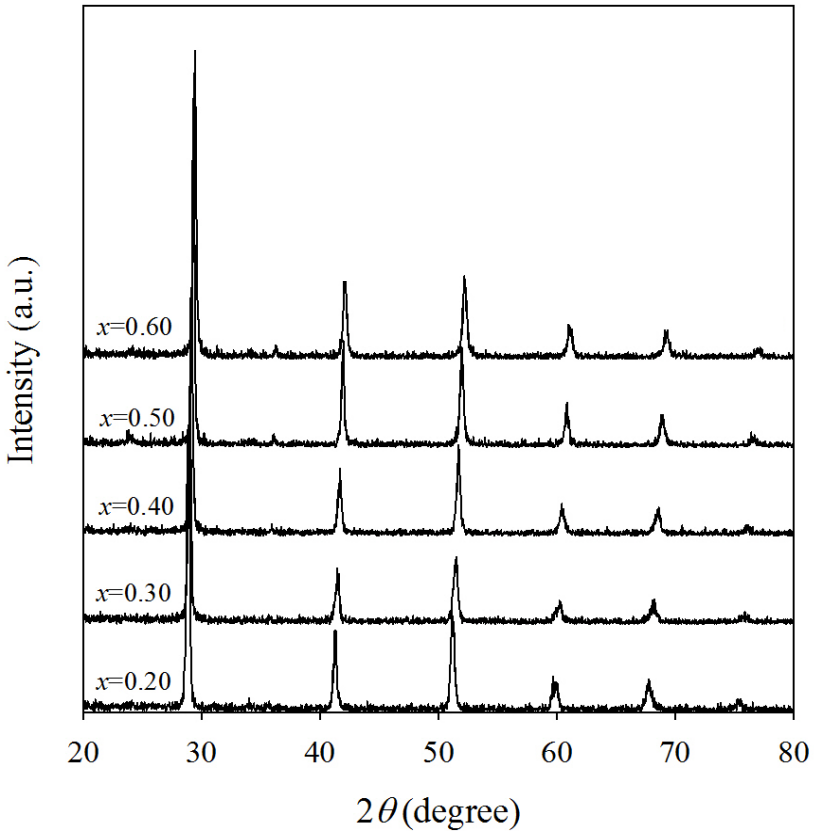

Figure 2: XRD pattern for $Ba(Ce_{1-x}Zr_x)_{0.95}Yb_{0.05}O_{2.975}$ after the samples in the form of disk were sintered at 1400-1450 ^oC

Particle size distribution

Particle size distribution for $Ba(Ce_{1-x}Zr_x)_{0.95}Yb_{0.05}O_{2.975}$ powders after calcined at 1100 ^oC is characterized by two groups namely loose powder and agglomerate. The loose particles are spherical in shape and have a diameter in the nanometer range (50-200 nm) as shown in Figure 3. The data obtained from scanning electron microscope (SEM) and particle analyzer for both groups are almost similar to each other as presented in Table 1.

As Zr-content increased, the loose powder become generally smaller and tends to form more agglomerates. The reason may be due to the contraction of the unit cell volume (V) as reported [10]. For smaller V, the particles become less charging and tend to form hard agglomerates. The incapability of particle analyzer to reveal loose powder for the sample x=0.40, 0.50 and 0.60 signified that the bulk samples are dominated by agglomerates as also reported by Taglieri et. al. [14].

Solid State Science and Technology, Vol. 19, No2 (2011) 80-91
ISSN 0128-7389

Table 1: Particle size of loose powder and agglomerate for $Ba(Ce_{1-x}Zr_x)_{0.95}Yb_{0.05}O_{2.975}$ samples obtained from particle analyzer and SEM

Sample	Loose powder (nm)		Agglomerate (nm)	
	SEM	Particle Analyzer	SEM	Particle Analyzer
x=0.20	70–200	100– 200	300–750	300–700
x=0.30	60–150	100– 200	200–500	300–500
x=0.40	60–100	–	150–450	200–500
x=0.50	60–100	–	150– 400	200–400
x=0.60	50–100	–	100–400	200–400

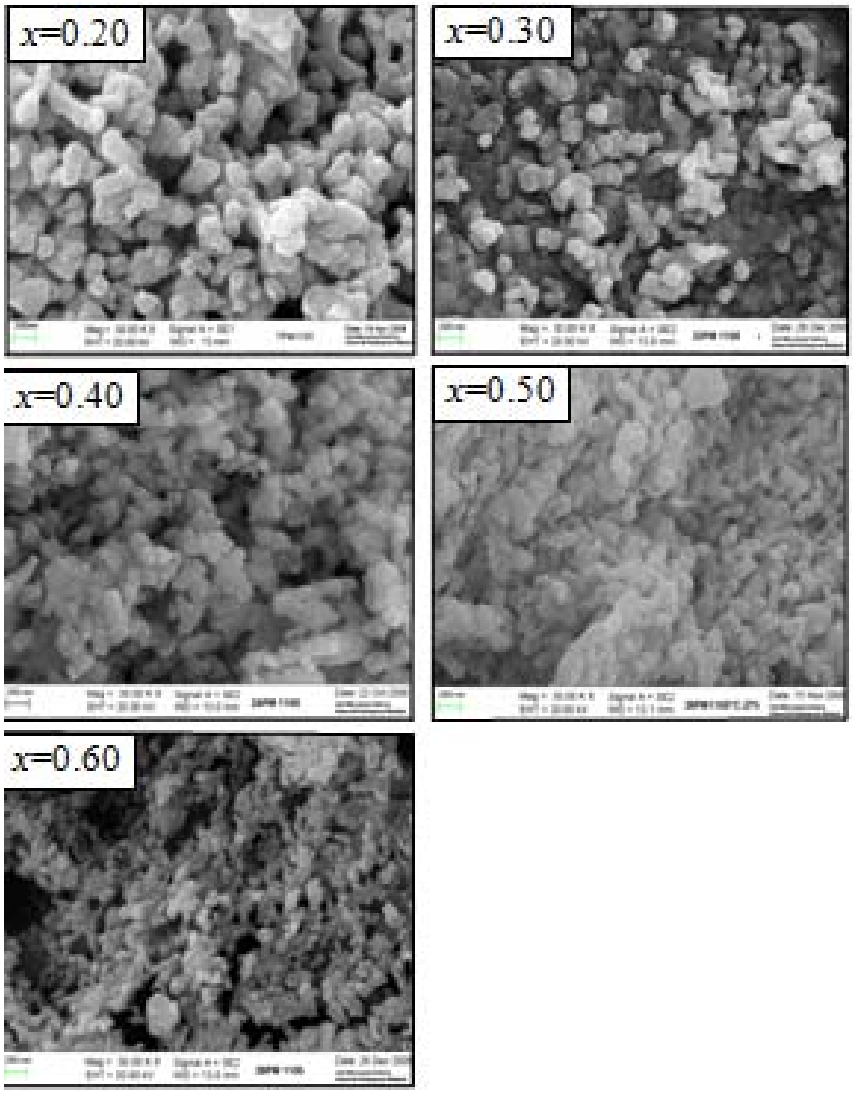

Figure 3: SEM images for the sample in form of powders with various Zr-content after calcined at 1100 ^{o}C

Solid State Science and Technology, Vol. 19, No2 (2011) 80-91
ISSN 0128-7389

Microstructure of sintered pellet

Table 2 shows the relative density of the samples at sintering temperature of 1400-1450 ^{o}C. Up to x=0.40, the desired temperature to obtain density of pellet to more than 90% is about 150-300 ^{o}C lower than those used in solid-state reaction (SSR) method [7,8,15]. The reduction in this sintering temperature can be ascribed to the enhanced kinetics due to the ultra-fine loose powders and small agglomerates. However, the relative density decreased as Zr-content increased. The reason may be due to the presence of hard agglomerates as discussed above. It is known that for hard agglomerates, higher sintering temperatures are required to get a dense ceramics material.

Table 2: Relative density for $Ba(Ce_{1-x}Zr_x)_{0.95}Yb_{0.05}O_{2.975}$

Sample	Relative density (%)
x=0.20	95.1
x=0.30	94.4
x=0.40	93.8
x=0.50	85.1
x=0.60	61.9

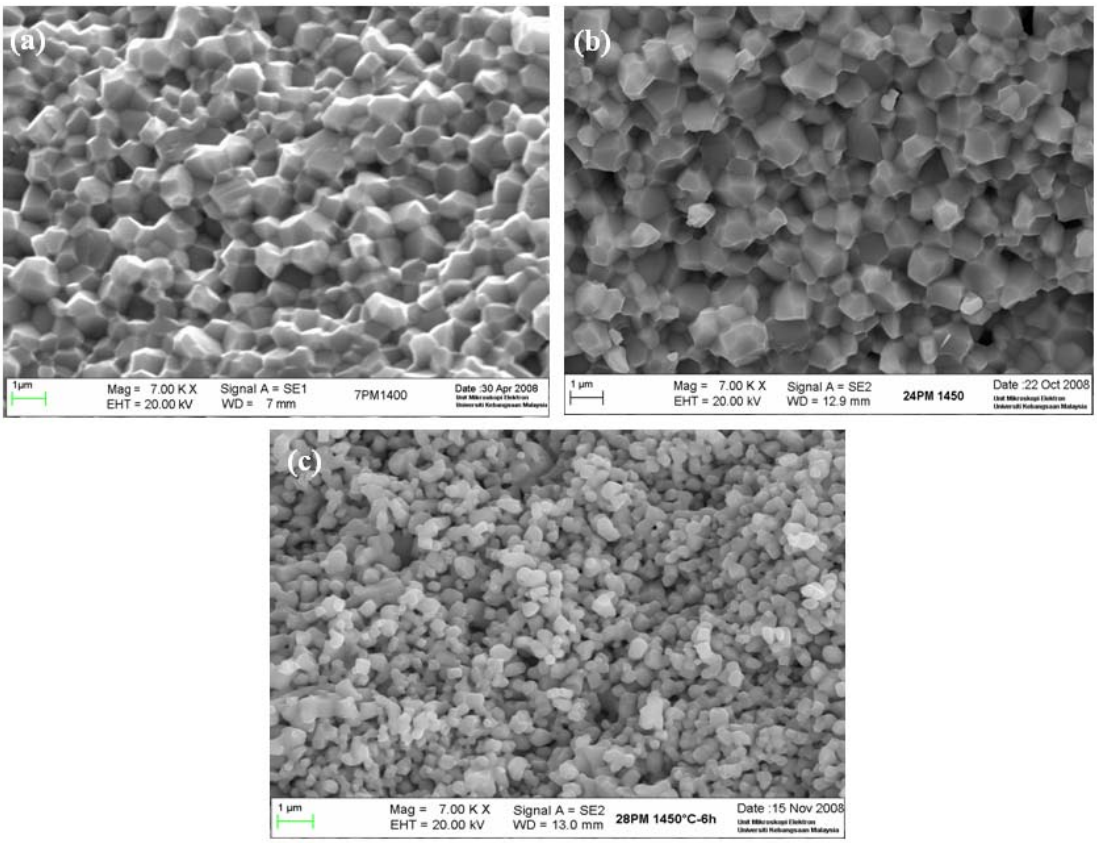

Figure 4: SEM micrographs showing the microstructure of the fracture surface of pellet for $Ba(Ce_{1-x}Zr_x)_{0.95}Yb_{0.05}O_{2.975}$. (a) x=0.20, (b) x=0.40 and (c) x=0.60

The dense samples (for example x=0.20 and x=0.40) exhibit well-defined grain formation compared to the x=0.60 as shown in Figure 4. The grain size for all samples is about 0.5 to 1.5 µm. Samples with x=0.50 and x=0.60 show smaller grain size and bigger pore size. The discrepancy in microstructure (such as grain and pore size) between dense and porous samples can be associated to the effect of size, amount and type of particle and agglomerate in the ceramics powder.

The relatively low sintering temperature obtained in this study for samples with x=0.20, 0.30 and 0.40 is still high in order to prevent the evaporation of BaO at the pellet surface. According to Magrez and Schober [13], during high-temperature processing (T>1250 ^{o}C), the vaporation of the BaO from the pellet surfaces could not be avoided. Therefore, we polished the pellet surfaces prior to XRD and conductivity measurements.

Electrical conductivity
By taking into account the trapping of air or any impurities inside the voids or pores in porous sample, only samples with x=0.20, x=0.30 and x=0.4 were chosen for the impedance measurements. The evolution of impedance arcs was observed as a function of temperature as recommended by Kreuer [16]. This is because the impedance analysis still suffers from a certain amount of ambiguity in this high conducting ceramics.

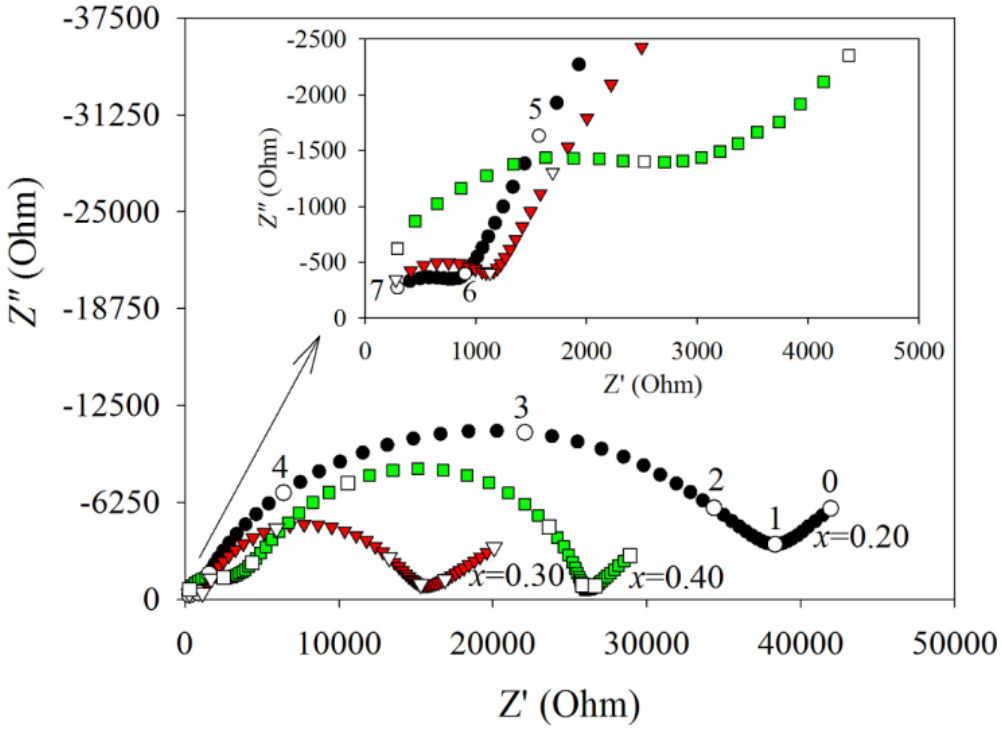

Figure 5: Impedance spectrum of $Ba(Ce_{1-x}Zr_x)_{0.95}Yb_{0.05}O_{2.975}$ at 250 ^{o}C in wet hydrogen (number 0 to 7 is n value for 10n in the frequency range of impedance measurement). The arcs are not geometrically corrected

At 200 ^{o}C, the high frequency arc corresponds to grain response and the mid-frequency arc is associated to the grain boundary response. The third arc is attributed to the electrode/electrolyte interface. An example for Nyquist plots for the samples at 250 ^{o}C is shown in Figure 5. Impedance spectra revealed that the grain semicircle was observed only at $T \leq 250$ ^{o}C. Up to 250 ^{o}C, the equivalent circuit consists of a combination of three parallel pairs of resistor-constant phase element in series.

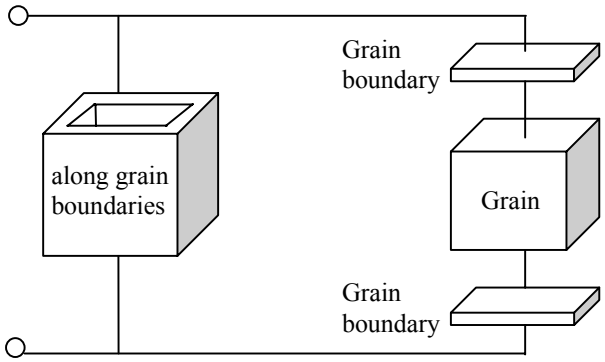

Figure 6: Brick Layer Model [18]

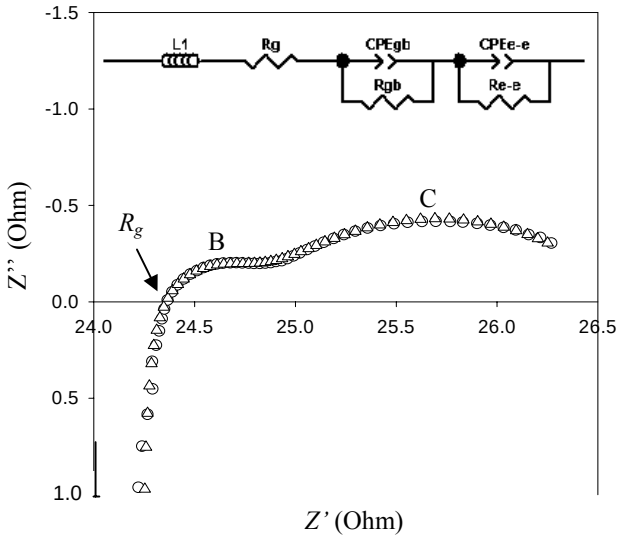

Figure 7: Impedance spectrum and an equivalent circuit of $Ba(Ce_{1-x}Zr_x)_{0.95}Yb_{0.05}O_{2.975}$; x=0.20 at 700 ^{o}C in wet hydrogen. (O) experimental data and (Δ) simulation data. B and C are the responses corresponded to the grain boundary and electrode/electrolyte interface

Above 300 ^{o}C, the grain resistance (R_g) was obtained from the intercept value of the grain boundary arc with the real axis at high frequency. It was also noticed that above

400 ^{o}C, the *Z*- imaginary data at high frequencies change its sign to positive values. The effect was due to the presence of inductive element caused by the experimental set-up [17]. As temperature increased, the inductive effect became dominant due to the smaller specimen resistance compared with the input impedance of the analyzer. This artifact limits the capability of Solartron 1260 frequency response analyzer at 32 MHz.

All the responses were resolved by the fitting procedure using an equivalent circuit representing the brick-layer model as shown in Figure 6. The fitting was done until the experimental and simulation data are almost completely superimposed as shown in Figure 7.

The relation of $C = Y^{1/n} R^{\left(1/n - 1\right)}$, where R is the resistance and Y and n is the parameters associated with the constant phase element (CPE), was used to calculate the capacitance value. Table 3 shows the geometrical capacitance value for the grain (C_g) and grain boundary (C_{gb}) responses of $Ba(Ce_{1-x}Zr_x)_{0.95}Yb_{0.05}O_{2.975}$; x=0.40 at selected temperatures (T). The identification of the first semicircle as bulk response based on the extracted capacitance was in the order of 10^{-12} to 10^{-11} farad. The capacity of the second semicircle was of the order of several nanofarad and corresponds to the grain boundary [19].

Table 3: Geometrical capacitance value for grain and grain boundary responses

T (^{o}C)	C_g (F)	C_{gb} (F)
200	2.1 x 10^{-11}	1.2 x 10^{-9}
250	2.4 x 10^{-11}	1.3 x 10^{-9}
400	-	0.8 x 10^{-9}
550	-	0.3 x 10^{-9}
600	-	0.4 x 10^{-9}

From the analysis of impedance spectrum, the R_g data points were found to deviate from the linearity of Arrhenius behavior. Thus, only total conduction was discussed in this study. The total conductivity (σ_T) was calculated from the total resistance (R_T): $R_T = R_g + R_{gb}$; where R_g is grain resistance; R_{gb} is grain boundary resistance and the bulk dimensions of the sample (t is thickness and A is surface area of the sample) as equation (1).

$$\sigma_T = \frac{t}{(R_T A)} \qquad (1)$$

Figure 8 shows the a.c. conductivity of samples in wet hydrogen at various temperatures. It is clearly seen that there are two temperature regimes for each sample namely at low temperatures (200- 450 ^{o}C) and intermediate temperatures (450- 800 ^{o}C). At intermediate temperatures, the samples showed high proton conductivity in wet hydrogen and their values were found to be comparable to that prepared by SSR [5]. The activation energy, E_a, was estimated from the gradient of this Arrhenius graph. The

E_a value for all samples in these temperature regimes is given in Table 4.

The higher E_a value at low temperature regime may be due to the grain boundary effect. There are many factors that contribute to the grain boundary resistance such as impurities segregation, grain size, pores and space charge. These factors particularly impurity phases, form a barrier and blockade to the charge carriers movement. Consequently, the samples exhibit low conductivity with high activation energy. As temperature increased, the charge carriers easily transfer or jump from one oxygen vacancy to the adjacent oxygen vacancy in lattice sites. Thus, it resulted to the high conductivity with low activation energy. At intermediate temperatures, the obtained E_a is almost similar to the activation energy for proton conductor as reported by Kreuer [16].

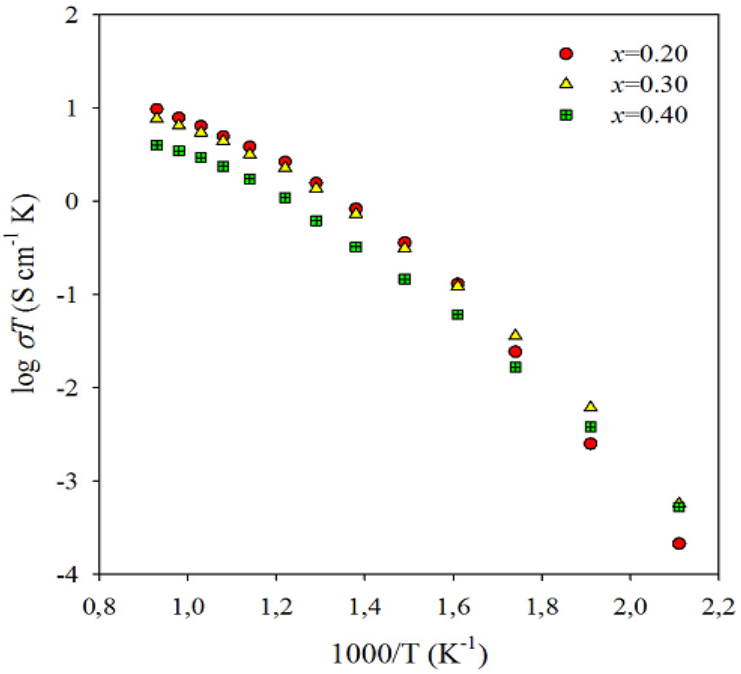

Figure 8: Total conductivity of $Ba(Ce_{1-x}Zr_x)_{0.95}Yb_{0.05}O_{2.975}$ as a function of temperature in wet hydrogen

Table 4: Activation energy for $Ba(Ce_{1-x}Zr_x)_{0.95}Yb_{0.05}O_{2.975}$ in wet hydrogen

Sample	E_a (eV) ($200 \leq T\,^oC \leq 450$)	E_a (eV) ($450 \leq T\,^oC \leq 800$)
x=0.20	1.00	0.46
x=0.30	0.81	0.41
x=0.40	0.73	0.39

CONCLUSION

$Ba(Ce_{1-x}Zr_x)_{0.95}Yb_{0.05}O_{2.975}$ solid solutions with different Zr-content were successfully prepared by a Pechini method. High purity of and dense samples for x=0.20, 0.30 and 0.40 were obtained at sintering temperature of 1400-1450 ^oC. Synthesis by this route produced small size particles. SEM observations indicate that the particles size of the solid solutions were about 50 to 200 nm. It was shown that the grain boundary resistance gave a higher contribution to the total resistance of samples. Due to the limitation of impedance spectroscopy measurement at $T \geq 300$ ^oC, thus, only total conduction was reported in this work. At 600 ^oC, the total conductivity of the sub-micron grains $Ba(Ce_{1-x}Zr_x)_{0.95}Yb_{0.05}O_{2.975}$ is 4.4 x 10^{-3} S cm^{-1} for x=0.20, 3.6 x 10^{-3} S cm^{-1} for x=0.30 and 2.0 x 10^{-3} S cm^{-1} for x=0.40.

ACKNOWLEDGEMENT

Nafisah Osman is grateful to Universiti Teknologi MARA for the PhD scholarship and sponsorship for attending the conference.

REFERENCES

[1] Y. Guo, R. Ran, and Z. Shao, *Inter. J. Hydrogen Energy*, **35** (2010) 5611-5620
[2] J. Zhang, Z. Wen, S. Huang,, J. Wu, J. Han, and X. Xu, *Ceramics International*, **34** (2008) 1273-1278,
[3] A.K. Azad, and J.T.S Irvine, *Solid State Ionics*, **178** (2007) 635-640.
[4] H. Iwahara, in B.V.R. Chowdari, and S. Radhakrishna, (editor.) *Solid State Ionics Devices*, (Singapore: World Scientific 1988), 289-307
[5] K. Katahira, Y. Kohchi, T. Shimura, and H. Iwahara, *Solid State Ionics*, **138** (2000) 91-98.
[6] J. Lv, L. Wang, D. Lei, H. Guo, and R.V. Kumar, *Journal of Alloys and Compounds*, **467** (2009) 376-382.
[7] S. Ricote, N. Bonanos, M.C. Marco de Lucas, and G. Caboche, *J Power Sources*, **193** (2009) 189-193
[8] K.H. Ryu, and S.M. Haile, *Solid State Ionics*, **125** (1999) 355-367.
[9] N. Osman, I. A. Talib, and H. A. Hamid, *Ionics*, **16** (2010) 561-569.
[10] N. Osman, "Pencirian Bahan Elektrolit Pepejal Berasaskan $Ba(Ce,Zr)O_3$ yang Didopkan dengan Yb^{3+} sebagai Bahan Konduktor Proton pada Suhu Pertengahan, ($400 \leq T\ ^oC \leq 750$)" (Ph.D. thesis, School of Applied Physics, Faculty Science & Technology, UKM, 2009)
[11] N. Osman, I. A. Talib, and H. A. Hamid, *Ionics*, **15** (2009) 203-208
[12] B. Robertz, F. Boschini, A. Rulmont, R. Cloots, I. Vandriessche, S. Hoste, and J. L. Beckers, *Journal of Materials Research*, **18** (2003) 1325-1332
[13] A. Magrez, and T. Schober, *Solid State Ionics*, **175** (2004) 585-588
[14] G. Taglieri, M. Tersigni, P.L. Villa, and C. Mondelli, *Inter. J. Inorg. Mater.*, **1** (1999) 103-110

[15] J. Li, J.L. Luo, K.T. Chuang, and A.R. Sanger, *Electrochimica Acta*, **53** (2008) 3701- 3707
[16] K.D. Kreuer, *Solid State Ionics*, **125** (1999) 285-302.
[17] M. Mogensen, T. Lindegaard, U.R. Hansen, and G Mogensen, *J. Electrochem. Soc.*, **141** (1994) 2122 – 2128,
[18] N.J. Kidner, B.J. Ingram, Z.J. Homrighaus, T.O. Mason, and E.J. Garboczi, (2003). *Proceedings of Solid-State Ionics 2002 (reprinted)*: pp. 756
[19] A.R Potter, and R.T. Baker, *Solid State Ionics*, **177** (2006) 1917-1924